Channel Reciprocity Analysis and Feedback Mechanism Design for Mobile Beamforming Systems

Yan Shi ⬤, Mahmoud Badi ⬤, Dinesh Rajan, *Senior Member, IEEE*, and Joseph Camp ⬤, *Member, IEEE*

Fig. 1.　Channel Feedback Mechanisms. (a) Explicit. (b) Implicit.

Abstract—Accurate channel state information (CSI) is essential to increasing throughput in multi-input, multi-output (MIMO) systems with digital beamforming. CSI can be acquired by channel estimation and reported via feedback mechanisms. While the training and feedback overhead are typically proportional to the number of antennas, uplink measurements can be utilized to predict downlink CSI assuming perfect channel reciprocity in a time division duplex (TDD) mode. However, many works make the assumption that channels are perfectly reciprocal, which is often not the case in practice due to poor channel estimation and physical channel asymmetry. In this work, we investigate the key challenges in channel feedback performance, including TX-RX imbalance, channel coherence, and interference for mobile systems. We evaluate IEEE 802.11ac-based implicit and explicit feedback schemes with both emulated and in-field MIMO channels, particularly in regards to drone-based transmissions. Our analysis with channel emulation shows that implicit feedback is susceptible to channel reciprocity errors, while explicit feedback is more sensitive to Doppler effects. We propose a hybrid feedback mechanism that increases the throughput by 32% over conventional feedback methods. We additionally evaluate the impact of frequency offset asymmetry on the performance of distributed mobile systems. Our in-field experiments demonstrate that explicit feedback can provide better throughput improvement than implicit feedback in highly-mobile air-to-ground channels. Since our study spans many critical frequency bands, these results serve as a fundamental step towards understanding the impacts of asymmetric factors of channel reciprocity for drone-based beamforming systems.

Index Terms—MIMO, UAVs, channel estimation.

I. INTRODUCTION

THE key to increasing the throughput of IEEE 802.11 networks is the design of robust and efficient channel feedback mechanisms with MIMO antennas. With the mobile wireless demands of users exploding in recent years, network operators have increasingly deployed multiple antenna systems to support the growing number of high-bandwidth streaming functionalities. Multiple antennas at the transmitter can perform spatial processing in order to support the growing number of multimedia functions targeted to user equipment (UE). This technology requires antenna coordination with the aid of CSI

feedback to direct beams for large data transmission. Channel reciprocity is an inherent property of TDD wireless systems, which predicts uplink (UL) and downlink (DL) channel knowledge from DL/UL channel measurements without additional feedback. In contrast, we focus on channel estimation and feedback mechanisms in TDD-based IEEE 802.11 systems to enhance the throughput.

Typical feedback mechanisms roughly fall into two categories for 802.11 networks: implicit feedback and explicit feedback [1]–[3], as shown in Figure 1. In 802.11ac explicit feedback, the transmitter first sends a null data packet (NDP) as a sounding/training frame to the UE in the downlink (DL) direction. After decoding the received signal, the UE performs channel estimation and sends back the compressed CSI to the transmitter [2]. Implicit feedback is first supported in 802.11n, where the transmitter implicitly obtains an estimate of the DL channel by taking the transpose of UL CSI, assuming that DL and UL channels are perfectly reciprocal [3]. Current explicit feedback mechanisms use compressed data representation that causes CSI mismatch and lacks flexibility to address practical non-ideal channel reciprocity issues. Frequency extrapolation methods for FDD downlink CSI acquisition have also been proposed for frequency division duplex (FDD) systems, where the impacts of feedback overhead and delay on channel reciprocity cannot be ignored [4]–[6]. A directional training and feedback scheme to perform frequency extrapolation of departure angles and number of dominant departures has been proposed [4] and achieved significant spectrum efficiency improvements over full training for FDD systems. An eigenspace channel estimation method with optimized CSI feedback codebooks and a judiciously-designed training sequence to achieve low dimensional channel estimation for FDD systems has been proposed in [5]. A super-resolution theory on synthetic channel models has also been established to achieve channel reciprocity in FDD systems [6].

Statistical models for predicting channel reciprocity error (CRE) have been proposed [7]–[14]. With perfect channel reciprocity, implicit feedback will incur less overhead and improve throughput performance. However, most of these works overlook the fact that, in practice, the DL and UL channels may not be reciprocal. The key factors that introduce non-ideal channel reciprocity and degrade the performance of implicit feedback include CRE caused by TX-RX imbalance [8]–[10], noise power difference [11], [12], as well as channel estimation error introduced by device movement [13], [14] or device-antenna interaction [15]. To the best of our knowledge, none of the current published works discuss the isolated and joint effects of CRE, channel coherence variation, and changing effective noise power on the feedback performance.

Lastly, we leverage our evaluation of drone-based mobile systems to investigate feedback protocols in a real-world context. The future development of airborne wireless communication necessitates precise channel characterization and MIMO support due to increasing deployments of aerial networks and their resulting data services. Theoretical studies have characterized DL air-to-ground channel estimation with theoretical simulations but lack experimental validation [16]–[20]. Although these works have simulated air-to-ground channels in urban environments, most of the aforementioned works lack channel reciprocity evaluation of explicit and implicit feedback for drone-based beamforming due to the assumptions inherently made within the simulation environment.

In this work, we quantify the impact of key factors that degrade the performance of IEEE 802.11ac MIMO techniques and feedback mechanisms, including CRE caused by transmitter-receiver imbalance, Doppler shifts related to the time-varying channel, and noise power divergence between transmitter and receiver. In particular, the Doppler shift is attributed to a channel that has a coherence time shorter than the OFDM training period, resulting in frequency shifts in the received OFDM symbols [12]. The performance of channel feedback is sensitive to CSI mismatch over the Doppler spread channels. The noise power can be modeled as an effective additive noise due to different interference power profiles between transmitters and receivers. For instance, in airborne communications, very different background noises, spatial separations, interference sources present between drone/unmanned aerial vehicle (UAV) in the air and ground station on the ground. Thus, the effective noise can greatly reduce the validation of channel estimation. Furthermore, we analyze the joint effects of CRE on feedback performance for centralized and distributed MIMO systems. Although CRE can be evaluated by both simulations and experiments, the impact of mobility is only addressed by simulations in current works [16]. To improve the system performance, we then propose novel feedback mechanisms which are robust to CRE and channel coherence. Lastly, we build an IEEE 802.11ac-based signaling mechanism across the media access control and physical layers to explore in-field beamforming (UAV-based transmissions), demonstrating that a properly optimized drone-based digital beamforming system can provide significant throughput improvements using explicit versus implicit feedback. In doing so, we perform in-depth experimental design and analysis on

resulting in-field data, which requires understanding numerous interacting complex sub-systems. These systems include multiple programmable RF chains and time-varying channels in both the uplink and downlink directions. In performing a series of experiments that help to first isolate the effects of various components and then jointly consider their effects, we evaluate existing and proposed channel feedback mechanisms in realistic and representative environments.

The main contributions of this paper are as follows:
1) We present the design of a novel explicit channel-differential feedback mechanism, which considers the difference between downlink training signals and their corresponding uplink response to reduce MIMO CSI feedback overhead and save computational complexity, while maintaining channel feedback accuracy.
2) We compare implicit and explicit feedback mechanisms by evaluating the key factors that degrade the feedback performance, including TX-RX imbalance, Doppler effects, and effective noise, showing that implicit feedback is susceptible to CRE, while explicit feedback is more susceptible to channel coherence.
3) We propose a hybrid feedback mechanism that is robust to both CRE and channel coherence on a channel emulator and demonstrate significant throughput performance improvement over the existing IEEE 802.11ac standard by 32%.
4) We conduct in-field experiments with programmable radios mounted on UAV platforms that realize air-to-ground beamformed communications to evaluate channel feedback performance in a realistic environment, showing channel feedback and estimation accuracy are largely affected by velocity and reciprocity errors.
5) We extend our design and evaluation to distributed MIMO systems, revealing the impact of relative frequency offsets and Doppler shifts on system performance.

The rest of the paper is organized as follows: We first discuss related work in Section II. In Section III, we propose channel-differential and hybrid feedback mechanism design. Then, we discuss the hardware setup for our feedback schemes in Section IV. In Section V and Section VI, we present our channel reciprocity measurements for both repeatable and realistic channel conditions on a channel emulator and in a representative environment, respectively. We conclude in Section VII.

II. RELATED WORK

This work has relevance across the following areas: (*i.*) Feedback Mechanisms, (*ii.*) Channel Reciprocity, and (*iii.*) Beamforming.

Feedback Mechanism: IEEE 802.11 standards specify two types of feedback mechanisms: implicit feedback and explicit feedback. Both IEEE 802.11ax and 802.11ac implement an explicit feedback scheme to calculate the optimal transmit diversity weights [2]. These channel feedback mechanisms are based on the Singular Value Decomposition (SVD) of the channel. However, this procedure can require a large computation cost [8].

While explicit feedback can provide more accurate CSI, it introduces large overhead in terms of time and feedback control bits. For implicit feedback, the transmitter does not need to measure and send the CSI to the beamformer. Implicit beamforming is also implemented 802.11n [3]. However, implicit beamforming requires frequent calibration between the transmitter and receiver when practical channels are not reciprocal, which can complicate the 802.11ac MIMO framework design [2].

Channel Reciprocity: In perfect channel reciprocity, implicit feedback will incur less overhead and improve throughput performance [7]–[14]. However, most works ignore the possibility that the channel is not perfectly reciprocal in practice. This is due to three reasons: signal path asymmetries between the transmitter and receiver, noise power asymmetries between the transmitter and receiver, and channel estimation error introduced by device movement. Channel reciprocity estimation inaccuracies due to TX-RX impairment has been fully discussed. For example, experiments have shown significant performance losses with implicit feedback due to non-reciprocity between the forward and reverse signal path when transceiver calibration is neglected [7]. Still other work has modeled the reciprocity error (gain mismatch) caused by the difference in transmit/receive analog front-end electronics under a narrow band assumption [8]. The different mutual coupling of transmitters and receivers, which can destroy the reciprocity in compact antenna array scenario, is also considered [9]. However, knowledge about the joint effects of channel reciprocity error and mobility on feedback performance is still lacking in current literature. Another work investigates the reciprocity error in OFDM systems and finds that the phase of reciprocity error rotates linearly in the frequency domain, which is caused by phase/amplitude imbalance between the transmitter and receiver [10]. Albeit insightful, this work only describes the phenomenon observed during experiments without further analysis of the internal cause and the impact of such OFDM-based phase errors on system link performance. Furthermore, the effective noise profile at the transmitter and receiver may be significantly different [11]. This causes the signal quality to be different between the forward and reverse link. A MMSE method has been proposed to minimize the demodulation error, assuming knowledge of the effective noise distribution [12]. The closest work to ours that investigates the impact of mobility on feedback performance is given by [13]. Channel reciprocity can theoretically be assumed for channels in which UL and DL transmissions share the same frequency spectrum and when the coherence time of the channel is much greater than the packet period. However, this is only true for channels with low Doppler spread [14]. In high mobility scenarios, we have observed frequency domain phase distortion and significant degradation with implicit channel feedback.

Beamforming: One of the key features for the next generation wireless standard development is the scaling of MIMO. Beamforming can improve the received signal strength of the intended user and reduce noise interference to unintended users [21], [22]. Beamforming architectures have been implemented on software-defined radio (SDR) testbeds using Universal Software Radio Peripheral (USRP) RF and baseband boards [7], [23], [24]. A wireless distributed beamforming system was built on an SDR platform [7]. The system design on an USRP-2922 prototyping for 5 G system beamforming/beamsteering is contained in [23]. A minimum variance beam steering algorithm has been proposed by [24] to demonstrate robust beamsteering capability on USRP. We consider our work to be the first to focus on the challenges associated with channel feedback and asymmetry caused by reciprocity errors in drone-based channels.

III. BEAMFORMING FRAMEWORK WITH CHANNEL RECIPROCITY AND FEEDBACK DESIGN

In this section, we introduce a beamforming framework with precoding and channel reciprocity models for TDD-based 802.11 wireless networks. We first examine the channel reciprocity model based on channel feedback and investigate how channel reciprocity is affected by the above mentioned factors. Then, we introduce our proposed channel feedback mechanisms that improve the performance.

A. Beamforming Framework

Consider a typical beamforming system with M transmit antennas at the access point and a single receive antenna on the UE side. The amplitude and phase of each RF chain at the transmitter can be digitally controlled.

Throughout this work, we use an IEEE 802.11 PHY frame structure for data transmission, which is composed of a preamble, header symbols, and payload symbols. At the k-th subcarrier, the same copies of independent and unit complex signal symbol $s(k)$ is coded by the beamformer prior to being sent to the UE from the m-th transmit antenna. Let K denote the total number of subcarriers of an OFDM structure. Considering a spatially-independent Rayleigh fading channel and assuming DL beamformed transmissions, the received signal $r(k)$ at the k-th subcarrier can be given as:

$$r(k) = \sum_{m=1}^{M} p_m h_{d,m}(k) w_m(k) s(k) + n(k) \qquad (1)$$

Here, p_m, $w_m(k)$, and $h_{d,m}(k)$ represent, respectively, the power scalar, normalized beamforming precoding vector, and DL channel coefficient in the frequency domain at the k-th subcarrier from the m-th transmit antenna. The complex Additive White Gaussian Noise with variance σ_n^2 is $n(k)$.

The estimated CSI can be obtained by transmitting known training symbols prior to frame decoding via either implicit or explicit feedback. In this work, we use a conjugate beamforming vector, described as [25]:

$$w_m(k) = \frac{\overline{h}_{d,m}(k)^*}{\|\overline{h}_{d,m}(k)\|} \qquad (2)$$

Here, $\overline{h}_{d,m}$ indicates channel coefficient estimates, and $*$ denotes the complex conjugate operator. Other parameters used in our testing system are shown in Table I. A list of channel-related abbreviations is given in Table II.

Parameters	Preamble	Data
Modulation Schemes	BPSK	BPSK/QPSK/64QAM
Total Subcarriers	52	52
Occupied Subcarriers	52	48
Pilot Subcarriers	0	4
FFT size	64	64
CP Interval	0.25	0.25

TABLE II
CHANNEL ABBREVIATIONS

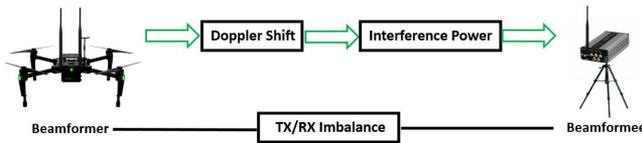| Symbol	Description
$\overline{h}_{d,m}$	DL channel coefficient estimate per antenna.
$\overline{h}_{u,m}$	UL channel coefficient estimate per antenna.
$h_{d,m}$	True DL channel coefficient per antenna.
$h_{u,m}$	True UL channel coefficient per antenna.
$\overline{h}_{b,m}$	Proposed hybrid channel estimates.
$\overline{h}_{i,m}$	Reconstructed channel estimate using the ith FIR filter tap.

Fig. 2. Feedback Analysis Scheme.

B. Channel Reciprocity Emulation Model

According to the literature discussed above, increasing the accuracy of the estimated channel $\overline{h}_{d,m}(k)$ is essential for the operational performance of the beamforming scheme. However, implicit feedback can never obtain perfect CSI due to the none-ideal reciprocity with imperfect channel estimation between the DL and UL channels and the induced Doppler effect due to mobility. There are three major contributing factors to reciprocity errors: TX-RX imbalance, effective noise power difference, and channels with Doppler effects. TX-RX imbalance is the mismatch between the transmit and receive RF chains of the same hardware device and the resulting amplitude/phase differences. In addition, mobility and noise introduce significant channel estimation error under different feedback schemes. However, few works model and quantify the joint effects of CRE and Doppler effects in terms of practical mobile MIMO systems.

The contributions of these key factors can be modeled by channel emulation with baseband pre-distortion, as shown in Figure 2. Specifically, RF impairments can be controlled by connecting the transmitter and receiver with an RF cable for synchronization and to compensate for phase differences. Then, baseband distortion can be modelled by multiplying the amplitude and phase shift in the baseband signal processing blocks to create controllable distortion levels. Finally, channel emulation is used to predict the UL channel information based on DL channel information as a function of frequency, mobile velocity, and propagation environments.

The systematic CRE introduced by the joint impacts of these key factors is given by:

$$h_{d,m}(k) = E(k)h_{u,m}(k) \qquad (3)$$

$$= e_{env}(k)e_{syn}(k)h_{u,m}(k) \qquad (4)$$

Here, $h_{d,m}(k)$ and $h_{u,m}(k)$ are the DL and UL channel fading coefficients, respectively. $E(k)$ is systematic CRE. The propagation reciprocity error component caused by TX-RX imbalance and channel estimation errors due to noise/interference is denoted by $e_{env}(k)$. Moreover, $e_{syn}(k)$ denotes the reciprocity error component introduced by imperfect synchronization between TX and RX. The lack of phase/frequency synchronization stems primarily from the frequency mismatch caused by Doppler effects, leading to phase rotation increasing linearly based on frequency [26].

Both TX-RX imbalance and noise will lead to amplitude and phase errors during channel estimation. Thus, the propagation reciprocity error introduced can be expressed as:

$$e_{env}(k) = A_m(k)e^{j\theta_m(k)} \qquad (5)$$

Here, $A_m(k)$ and $\theta_m(k)$ are modeled as normally-distributed and uniformly-distributed random variables, respectively. The synchronization reciprocity error e_{syn} due to the subcarrier-based phase rotation can be expressed as [26]:

$$e_{syn}(k) = e^{j\frac{4\pi k\delta_p}{K}} \qquad (6)$$

Here, δ_p is the slope of the phase error denoted by the phase gradient due to the Doppler shift's impact on phase distortion.

Following the above discussion, systematic CRE $E(k)$ is equivalent to:

$$E(k) = A_m(k)e^{j(\theta_m + \frac{4\pi k\delta_p}{K})} \qquad (7)$$

The issue of channel reciprocity is complicated by frequency and timing mismatch uncertainty when different nodes are equipped with independent local oscillators (LOs), resulting in asymmetric synchronization. If the relative frequency offset due to the LO frequency mismatch between transmitter and receiver is denoted as Δf. Then, the resulting constant phase rotation rate, based on accumulated phase time starting from the first OFDM symbol, is $4\pi\Delta f$. If we consider a phase conjugation relationship among DL/UL, then the phase rotation $\theta_m(n)$ at dedicated OFDM symbol t can be modeled as:

$$\theta_m(t) = e^{j\left(\frac{4\pi(t(K+K_{cp})+K_{cp})\Delta f}{Kf_{scs}}\right)} \qquad (8)$$

Here, t is zero-base OFDM symbol index which is known at transmitter and receiver, K_{cp} is the cyclic prefix duration, and f_{scs} is the OFDM subcarrier spacing. The accumulated time considers the previous t OFDM symbols after CP removal in the current symbol. Therefore, for distributed MIMO systems, the equation describing CRE (7) will become [13]:

$$E(k) = A_m(k)e^{j\left(\frac{4\pi(t(K+K_{cp})+K_{cp})\Delta f}{Kf_{scs}} + \frac{4\pi k\delta_p}{K}\right)} \qquad (9)$$

The estimated CSI can be obtained by transmitting known training symbols via either implicit or explicit feedback.

C. Channel-Differential Explicit Feedback Mechanism

In the current 802.11ac, large feedback overhead or mismatched CSI will greatly degrade the MIMO transmissions [2]. The transmitter first sends training frames to the UE, while the UE sends back the compressed CSI after decoding the training
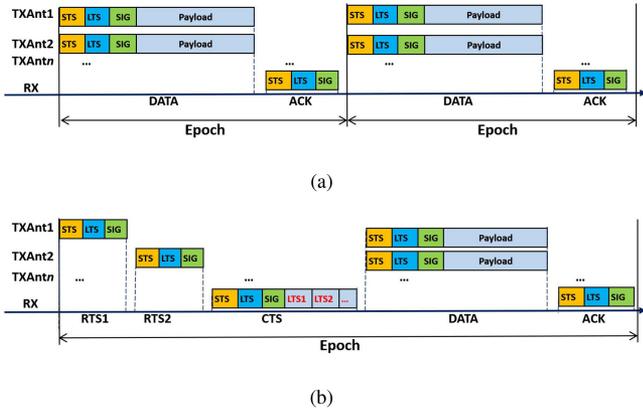
(a)

(b)

Fig. 3. Schematic diagram of epoch of 802.11ac-based feedback mechanisms: (a) Implicit and (b) Explicit.

frames. Existing works have focused on the precoder codebook to choose the matrix index [27]–[30]. In these works, the receiver needs to compress the CSI and prepare the feedback with extra computational cost. We propose an approach that expedites CSI feedback by eliminating CSI processing at the receiver with a relay procedure.

Figure 3(a) illustrates implicit transmission epochs with 2 transmit antennas in 802.11ac. The receiver sends the sounding NDP frame to the transmitter that serves two purposes: to acknowledge the previous epoch transmission and to perform UL channel estimation for the next transmission epoch. The NDP only includes a general 802.11 PHY preamble frame that consists of a short training sequence (STS) followed by a long training sequence (LTS) and the signal field (SIG). The timeline of our proposed channel-differential feedback method based on IEEE 802.11ac explicit feedback is shown in Figure 3(b). In each epoch, CSI information is "relayed" to the transmitter by fully eliminating CSI processing at the receiver, which greatly expedites the feedback as well as limits power consumption. In particular, the transmitting antenna takes turns sending M sounding frames (NDPs) to the receiver. Instead of performing CSI estimation on these received messages, the receiver appends the received LTS OFDM symbols to the end of the feedback message without modification before sending back. Note that the feedback contains $(M+1)$ LTSs, in which M LTSs have been processed in the DL direction and one original LTS in the preamble afterward. When the receiver sends back the feedback, all the LTSs are then processed by the UL path. The received symbol $r_{pre}(k)$ derived from the preamble LTS directly sent from UE at k-th subcarrier per training antenna is given by:

$$r_{pre}(k) = p_m h_{u,m}(k)s(k) + n_u(k) \quad (10)$$

The received symbol $r_{rel}(k)$ for the m-th relayed LTS propagating through DL and then UL channels is given by:

$$r_{rel}(k) = p_m h_{u,m}(k)h_{d,m}(k)s(k) + h_{u,m}(k)n_d(k) + n_u(k) \quad (11)$$

Here, $n_d(k)$ and $n_u(k)$ denote the DL and UL additive noise, respectively. Assuming noise and DL/UL CSI are statistically-independent and follow AWGN distribution, dividing the expectation of $r_{pre}(k)$ by $r_{rel}(k)$ gives the channel coefficient difference:

$$\frac{E[r_{rel}(k)]}{E[r_{pre}(k)]} \quad (12)$$

$$= \frac{E[p_m h_{d,m}(k)h_{u,m}(k)s(k) + h_{u,m}(k)n_d(k) + n_u(k)]}{E[p_m h_{u,m}(k)s(k) + n_d(k)]} \quad (13)$$

$$= \frac{E[p_m h_{d,m}(k)h_{u,m}(k)s(k) + h_{u,m}(k)n_d(k)]}{E[p_m h_{u,m}(k)s(k)]} \quad (14)$$

$$= E[h_{d,m}(k)] - \frac{E[h_{u,m}(k)n_d(k)]}{E[p_m h_{u,m}(k)s(k)]} \quad (15)$$

Since the noise variable is independent from channel information across frame transmissions, we have in 15:

$$E[h_{u,m}(k)n_d(k)] = 0 \quad (16)$$

Therefore, the channel coefficient estimates for DL per training antenna is given by:

$$\overline{h}_{d,m}(k) = E[h_{d,m}(k)] - \frac{E[h_{u,m}(k)n_d(k)]}{E[p_m h_{u,m}(k)s(k)]} \quad (17)$$

$$= E[h_{d,m}(k)] \quad (18)$$

DL CSI can be assumed to be accurately derived using our proposed channel-differential method. Therefore, the data symbols may be precoded at the transmitter prior to being sent to the receiver.

In our previous work [25], we performed simulations of BER vs. SNR on a beamforming system by employing our proposed Channel-differential explicit Feedback approach and compared our proposed channel-differential feedback scheme with recent compression-based feedback mechanisms, showing a BER improvement of 1.63 dB over K-means Clustering and 2.35 dB over Vector Quantization under controlled simulated channels and identical transmission power. In this work, we additionally evaluate the computational cost of different feedback approaches across a diverse number of training subcarriers by counting how many mathematical operations are performed at the receiver in each scenario. Assume I and Q are 16-bit fixed point values before CSI compression and $K = 10$ for the K-means Clustering method. Using our proposed method, since only I and Q division is needed at the receiver, the number of mathematical operations will scale by 2 times the number of subcarriers. With K-means clustering, however, the subcarriers are divided into K clusters, then, the mean of each cluster is used to feed K compressed CSIs back to the transmitter. With the G-subspace Codebook Index method, assuming a binary search on I and Q, the cost will scale by $\log_2$(number of subcarriers) multiplied by 2 times the number of subcarriers. If the Vector Quantization method is used, compression is performed on the I and Q samples resulting in more operations compared to the other schemes. The results of the explained computational cost are plotted in Fig. 4. We observe that, as the number training OFDM subcarrier
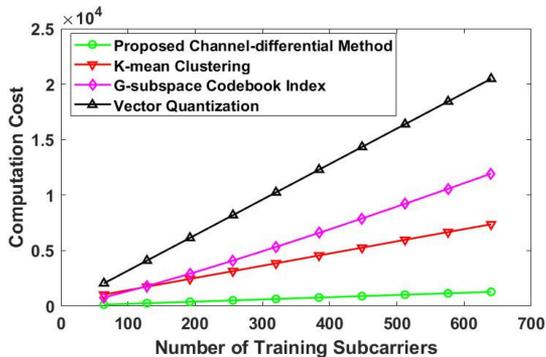
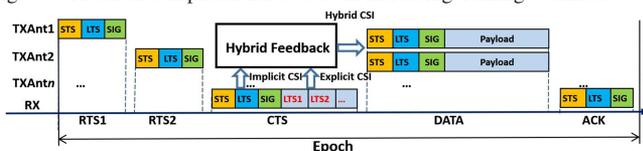Fig. 4.   Receiver computational cost at an increasing training overhead.

Fig. 5.   Schematic diagram of hybrid feedback mechanism.

(pilots) increases, our proposed approach maintains very low computational cost by offloading the computational burden to the transmitter and eliminating the need to perform compression and sourcing operations.

D. Hybrid Feedback Mechanism

In this part, we set forth a framework to construct a novel feedback mechanism that combines channel estimates obtained from both implicit and explicit feedback to improve the channel estimation accuracy.

As depicted in Figure 5, we consider implementing explicit feedback using the channel-differential protocol previously described. Additionally, implicit CSI can also be acquired from feedback or messages that make use of known preambles across the UL channel. Channel coherence can be estimated through the obtained channel impulse response and delay spread. CRE can be known by sending a training overhead in both the UL and DL channels. Both channel coherence and CRE will decide how implicit and explicit CSI jointly impact our hybrid channel estimation, denoted as $\overline{h}_{b,m}(k)$, which is given by:

$$\overline{h}_{b,m}(k) = \alpha \overline{h}_{d,m}(k) + (1 - \alpha)\overline{h}_{u,m}(k) \tag{19}$$

Here, α is the factor parameter that decides the ratio by which to distribute the contribution between implicit and explicit CSI, improving channel estimation accuracy. Note that $\overline{h}_{d,m}(k)$ and $\overline{h}_{u,m}$ are the DL and UL channel estimates per subcarrier k, respectively.

We first investigate the impact of α with a wide range of α options ($\alpha \in \{0.1, 0.3, 0.5, 0.7, 0.9\}$) to study and compare the performance of hybrid feedback with implicit/explicit feedback methods using emulated channels. For example, a ratio parameter α with a fixed value of 0.5 means equal contribution from both schemes. We also explore the throughput gain of each α value to find the best option using emulated channels. In practice, the Doppler frequency can be obtained by velocity measurements, while the CRE can be estimated using periodic training frames.
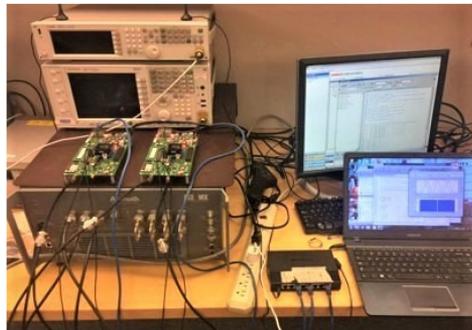

Fig. 6.   Experimental Setup with two WARP boards and an Azimuth Wireless Channel Emulator.

The combination of implicit and explicit feedback enables our hybrid feedback scheme to significantly improve channel estimation accuracy with known information of channel coherence and CRE. The ratio parameter can be indicated in the reserved field of the 802.11ac VHT-SIG field to support and initialize the hybrid feedback mode.

IV. HARDWARE SETUP

In this section, we first describe the design of our channel evaluation and outline the main factors that impact channel reciprocity. We then discuss our UAV-based beamforming framework that allows CSI feedback in our mobile system.

A. Channel Emulation Platform

We evaluate CRE using a software-defined radio platform and WARPLab with a channel emulator. WARPLab enables users to implement OFDM functionalities in MATLAB and encode/decode actual signals using synchronized radios [31]. Then, the coded and modulated data samples are transferred to the WARP board via an Ethernet cable. WARP is then triggered to transmit data samples over the air. The receiver samples the received signal over the air and then transfers the raw samples to the PC, where the receiver also leverages MATLAB to process the received data. During our experiments, one WARP board with two antennas acts as the beamformer/transmitter with precoding, and the other WARP board acts as a client device that is equipped with one antenna as a beamformee/receiver. We use an Azimuth Wireless Channel Emulator and Director II software to investigate the factors that affect the system performance [32]. The channel emulator can be controlled by TCL (Tool Command Language) scripts that generates controllable and repeatable channel conditions as a function of carrier frequency, Doppler shift, and scenario type for complex wireless environments. The hardware setup, for this channel emulation is shown in Figure 6.

In addition to the experimental setup, we evaluate the system with isolated factors and then their joint effects on feedback performance. We include a reference result which has no CRE error as the baseline case for our evaluation. The transmit signal bandwidth is 20 MHz, which is the maximum bandwidth supported by the WARP. We use an OFDM scheme with 64 sub-carriers on 5 GHz carrier frequency in our experiments.
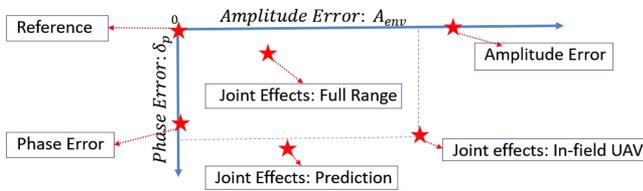
Fig. 7. RF mismatch for transceiver paths.
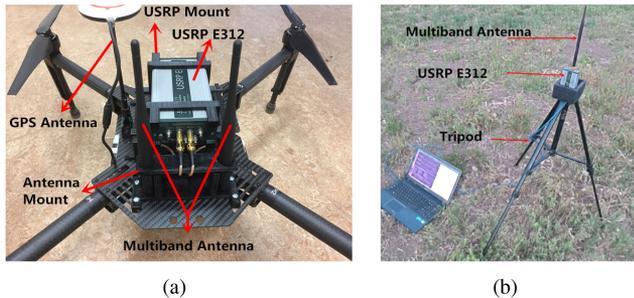

(a)   (b)

Fig. 8. Equipment settings for experiments. (a) Beamformer USRP mounted on a drone (b) UE USRP mounted on a tripod.
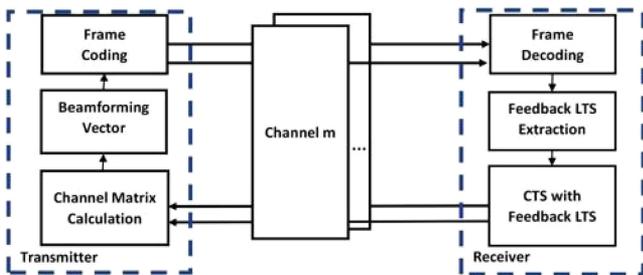

Fig. 9. State diagram of proposed beamforming transmission.

The experimental approach of our proposed CRE evaluation is shown in Figure 7.

B. Drone-Based Beamforming System

To build drone-based beamforming experimentation, we have designed and printed mounts for an Ettus E312 and two antennas to be secured on a DJI Matrice 100 (1-kg load capability), as shown in Figure 8. To do so, we have used a ROBO 3D printer and CAD software to ensure that a 10-cm separation exists between two antennas for diversity purposes and to allow for repeatability in testing by positioning them at the same location throughout all experiments. A dual-band VERT900 omni-directional antenna was used in the 900 MHz and 1800 MHz carrier frequencies; VERT2450 antennas were used for the 5 GHz experiments. Both antenna types provide a gain of 3 dBi. The receiver configuration is matched in terms of E312 hardware and is housed on a tripod at a height of 1 m above the ground.

We have designed and implemented PHY and MAC layers that carry out an IEEE 802.11ac-like channel feedback signaling using GNU Radio [33], [34]. The software state machine that describes our proposed beamforming testbed is shown in Figure 9. The digital samples are processed by Python signal processing blocks running on a Linux-based laptop. The path loss and

throughput are evaluated as a function of various horizontal distances and altitudes.

Our experiments are conducted over three carrier frequencies: 900 MHz, 1800 MHz, and 5 GHz. At the PHY layer, we use the same transmission epochs as the channel emulation platform described in Figure 3. We measure both BER and throughput to evaluate the beamforming system performance. While many works use the Shannon Capacity to map the SNR or BER to the ideal information rate [35], for a practical frame-based system, the throughput depends closely on the hand-shaking overheads and successful decoding of the received frames. In our work, link throughput (Mbps) is obtained by the bit error rate (BER) statistics, number of successfully recovered packets (N_s), and total transmission time (T) at each experiment, and calculated by the following equation:

$$Throughput = \frac{L_{pld} * B * N_s * (1 - BER)}{T} \quad (20)$$

Here, L_{pld} is the payload size in bytes carried by beamforming frame after channel estimation and feedback. B means 8 bits per byte.

V. SYSTEM ANALYSIS WITH CHANNEL EMULATION

Current IEEE 802.11 standards adopt a single feedback scheme, which inherently could be beneficial in some scenarios and inefficient in others. In this section, we quantify the effect of key factors on channel feedback mechanisms for 802.11ac beamforming precoding, including transmitter-receiver imbalance, Doppler effects, and effective noise power. We additionally evaluate the joint effect of these factors on centralized and distributed beamforming networks to approach practical transmission scenarios.

A. Impact of TX-RX Imbalance

We refer to TX-RX imbalance as the error in terms of amplitude and phase, stemming from the reliance on the transmitter and receiver chain difference without channel impacts. To study the impact of phase error on system link performance, the null data packet (NDP) sounding frames are sent bi-directionally with a constant channel attenuation of 70 dB to simulate the propagation path loss. Automatic gain control (AGC) is turned off during the experiments to ensure control of this attenuation. The channel is modeled as a Rayleigh fading channel with 5 taps that we embed in our channel emulation scripts. For each test, we fix the channel amplitude to be the same for DL and UL channels and measure the throughput as a result of changing the phase error percentage by increasing it from 0 to 80%. The throughput is calculated based on Equation (20).

Figure 10(a) presents the resulting throughput for various phase error percentages. The phase percent error is denoted as the ratio of error deviation compared to the recorded reference channel taps. In this plot, we can observe that with two transmit antennas, the implicit feedback incurs less overhead and improves throughput performance by up to 61% with no phase error. This link performance difference between explicit and implicit feedback is explained by the explicit overhead directly.
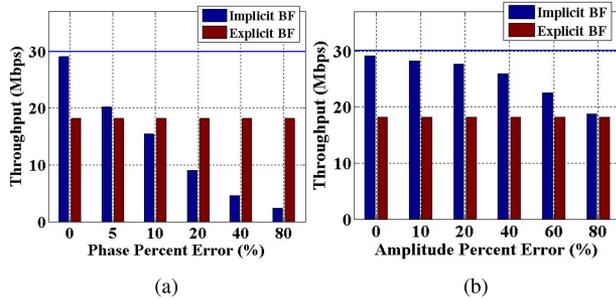
Fig. 10. TX-RX Imbalance Evaluation. (a) Throughput vs. Phase Error Percentage, and (b) Throughput vs. Amplitude Error Percentage.

Fig. 11. TX-RX Imbalance Evaluation: Throughput vs. Joint Amplitude and Phase Errors .

However, the performance of implicit feedback degrades sharply as phase error increases. For example, when we increase the phase error to approximately 80% we find that the throughput of implicit feedback would be less than 3 Mbps. This is for the fixed bandwidth of 20 MHz at a carrier frequency of 5 GHz. If the bandwidth is increased (*e.g.*, 160 MHz, as in 802.11ac/ax, 1.76 GHz, as in 802.11ad), the transmitted signal becomes more susceptible to the potentially destructive effects of fading such as phase dispersion and frequency-selective fading. In addition, from a hardware complexity perspective, the analog-to-digital converter can be easily saturated by the large amount of sampled and quantized signals, leading to delay and jitter in baseband processing. As a result, severe channel estimation errors and channel reciprocity degradation occurs in contrast to more narrow bands. If, however, narrow-band signals are in use, these effects are negligible as the signal experiences flat fading where all of its components are attenuated, phase shifted, and time delayed by approximately the same amount. In the narrow-band case, delays in baseband processing are minimal.

To quantify the impact of amplitude error, we repeat the experiments with a fixed phase error and evaluate the link throughput performance across different amplitude error percentages. The amplitude percent error is denoted as the ratio of error deviation compared to the amplitude of recorded reference channel taps. As shown in Figure 10(b), we observe implicit feedback stays almost the same in terms of performance as amplitude error increases and then degrades more sharply from 29.3 Mbps to 18 Mbps (as the amplitude error reaches the 60% to 80% range). Since the amplitude error percentage is found to be less than 20% in the large majority (95%) of practical instances in Section VI-A, the effect of amplitude error is far less significant as compared to phase error.

To examine the joint effect of phase and amplitude error on link performance, we fix the error value of one factor and change the value of the other factor for each experimental condition. The result is shown in Figure 11, where we use the same repeatable 5-tap, equal-power Rayleigh distribution model for this experiment via channel emulation scripts. We observe that, in a relatively good channel reciprocity condition, implicit feedback can outperform explicit feedback, by 21% on average. This is due to the advantage of saving overhead with implicit feedback (and relying on channel reciprocity) compared to explicit feedback with the same time-domain resources. Phase error, on the other
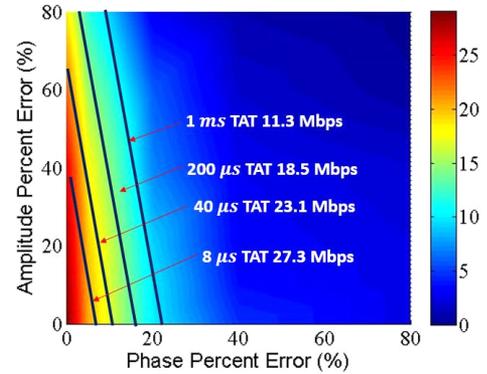
hand, has a more significant impact on system performance. This is explained by the performance separation curve that varies more severely along the phase axis. The separation curve is calibrated by different TX-RX switching times and based on our platform to investigate the performance of the different commercial transmitters. Our calibrated switching time rises from 8 μs to 1 ms. Since we use the WARP platform for experimentation in this section, we use a TX-RX switch time of 200 μs.

B. Impact of Doppler Effect

We now seek to enhance and extend current works on the evaluation of diverse feedback mechanisms in the presence of mobility. In particular, we evaluate the link performance of beamformed transmissions using the aforementioned experimentation setup for the emulated channel by introducing various levels of Doppler effects at a carrier frequency of 5 GHz. We use a channel emulator with a 3GPP R36 5-tap Rayleigh distribution model, which is typical for small cell coverage with NLOS conditions (*e.g.*, an auditorium, playground, or open-roof stadium). By implementing the Rayleigh fading model, the coherence time can be approximated by:

$$t_c = \frac{9}{16\pi f_d}. \tag{21}$$

Here, f_d represents the Doppler frequency shift given by $\frac{v f_c}{c}$.

High device mobility is known to affect channel estimation and feedback performance. In channel emulation, we use a central carrier frequency of 5 GHz for channel emulation. We vary the UE velocity to create different Doppler effects over the channel. Moreover, we use IEEE 802.11ac implicit feedback as a comparison to the performance of different channel feedback approaches. In order to consider the system performance at low and high velocity scenarios, we increase the velocity to 100 m/s across the various emulated channels.

1) Characterization of Doppler Effect: Figure 12 depicts how throughput decreases as Doppler frequency increases, an effect which is induced by mobility. For each test, we repeatedly send 10 k frames and analyze the successfully decoded payload in one second, which is interpreted as throughput. The results are shown for both explicit and implicit feedback schemes. The
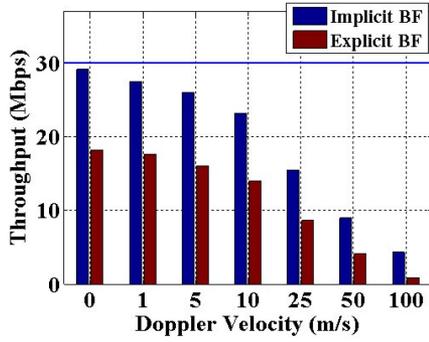
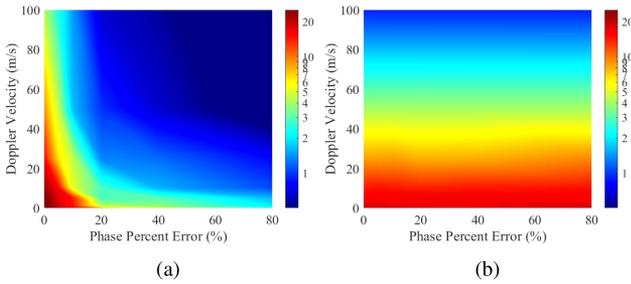Fig. 12.   Doppler Effect Evaluation: Throughput vs. UE Velocities.

Fig. 13.   Doppler Effect Evaluation: Throughput Performance vs. Changing Velocities. (a) Implicit. (b) Explicit.

theoretical throughput (the blue line on the y-axis) is based on 64-QAM, considering a training overhead of 10 ms. We observe that, by increasing the emulated Doppler velocity from 0 to 100 m/s, throughput in both feedback schemes decreases by 85%. However, the throughput of the implicit feedback scheme degrades more severely than with explicit feedback. Furthermore, the peak throughput of implicit feedback when no Doppler shift is applied can, on average, reach 28.9 Mbps, which means the predicted value is very close to the theoretical throughput reference of 30 Mbps. Our evaluation demonstrates that it is necessary to eliminate phase error to improve channel estimation.

2) Joint Effects of Doppler Effect and Phase Error: We present the throughput performance of the beamforming techniques based on explicit and implicit feedback schemes, as illustrated in Figure 13(a) and Figure 13(b), respectively. We observe that, for a fixed phase error, an increase in Doppler velocity significantly reduces the estimated throughput. For example, at a phase error of 20%, the Doppler effect reduces throughput by 60 to 90 percent beyond a velocity of 20 m/s. With the largest velocity setting, 100 m/s, the impact of less channel coherence introduced by mobility becomes stronger, resulting in less throughput with implicit feedback. However, for explicit feedback, the performance degrades more slowly compared to the implicit feedback scheme. This is explained by the fact that explicit feedback is robust enough to combat CRE by its capability to obtain accurate CSI in the DL direction. Thus, we can conclude that implicit feedback is more susceptible to the impact of reduced channel coherence.

3) Characterization of Channel Accuracy: Prompt and accurate channel feedback is essential for robust beamforming
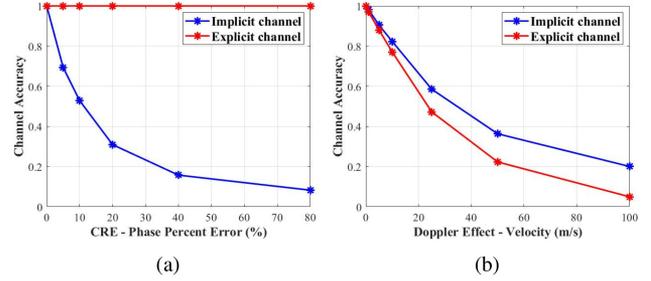

Fig. 14.   Channel Accuracy Analysis for implicit/explicit feedback. (a) Impact of CRE (Phase Error). (b) Impact of Doppler Effect.

design. In this part, we compare the performance of explicit and implicit channel accuracy by excluding the impact of overhead. The channel accuracy is characterized by comparing the configured channel vectors with estimated channel estimates. We first calibrate the recorded channel vectors provided by channel emulation at different levels of Doppler velocities and phase errors. Then, we evaluate the accuracy of the estimated channel of both feedback schemes. The channel accuracy is based on normalized MSE and given by:

$$\delta = 1 - \frac{1}{M} \sum_m^M \frac{\|\overline{\mathbf{h}}_\mathbf{m} - \mathbf{h}_\mathbf{m}\|^2}{\|\mathbf{h}_\mathbf{m}\|}. \tag{22}$$

Here, $\overline{\mathbf{h}}_\mathbf{m}$ and $\mathbf{h}_\mathbf{m}$ are the estimated channel vectors and pre-configured channel vectors for reference, respectively.

Figure 14(a) shows how channel estimation accuracy changes with increasing phase errors introduced over the emulated UL channel by comparing the estimates of explicit and implicit feedback schemes. The channel accuracy is an average estimation over 20 k transmission epochs (as shown in Figure 3) at each phase error condition. The estimated SNR during our experiments is as high as 53 dB, considering only thermal noise. By comparing both feedback schemes under the same condition and isolating the overhead for explicit, we observe that explicit feedback can perfectly capture the DL channel information with an estimation accuracy approaching 1. However, the estimation accuracy of implicit feedback, due to CRE, decreases from 1 to 0.12 as phase errors increase, which means that implicit feedback is highly susceptible to CRE.

Figure 14(b) shows the impact of increasing Doppler velocity on channel accuracy using both feedback schemes. Although a Doppler velocity of 100 m/s can introduce a Doppler frequency of 1.7 kHz in the emulated channel model, it has less impact on implicit feedback than explicit feedback. For example, the accuracy of implicit feedback decreases by 80%, while explicit feedback decreases by around 95%. *Of particular note in our evaluation is that implicit feedback is susceptible to CRE, while explicit feedback is more affected by Doppler effects.* This motivates the need for a hybrid feedback scheme that could make use of either scheme at the appropriate time according to the most favorable channel factor for that scheme. By further increasing the Doppler velocities, the performance degradation of channel estimation decreases gradually.
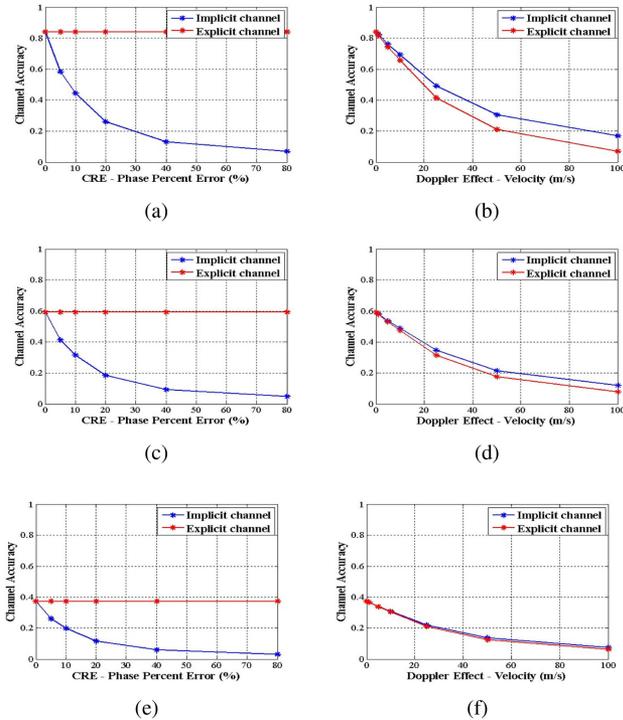
Fig. 15.　Effective noise Impact Analysis (a)(b) SNR = 8 dB (c)(d) SNR = 4 dB (e) SNR = 2 dB.

Fig. 16.　Channel Accuracy Analysis for Hybrid feedback. (a) Impact of CRE (Phase Error). (b) Impact of Doppler Effect.

C.　Impact of Effective Noise

Now, we explore the impact of co-channel noise power on the performance of channel estimation to anticipate similar effects in practical channels. To do so, we extract and compare the channel estimates based on transmissions of NDP sounding frames with various levels of the signal-to-noise ratio (SNR) applied to the receiver. The effective noise denotes the joint impact of interference power and thermal noise. By varying the values of p_i, we can emulate different noise power profiles between the transmitter and receiver and evaluate our system under different SNRs.

Figure 15 depicts channel estimation accuracy for implicit and explicit feedback with 6 different groups of SNR values. There are two interesting findings from these results: (i) The effects of Doppler velocity and phase error are clearly the most dominant at high SNR values, and (ii) Implicit and explicit schemes result in approximately the same performance under the impact of Doppler effects with low SNR values. These curves infer significant performance degradation of implicit feedback under low SNR values.

D.　Performance Evaluation of Hybrid Feedback Mechanism

In this part, we discuss the performance of our hybrid feedback mechanism that combines channel estimates obtained from both implicit and explicit feedback to improve the channel accuracy. We first evaluate the channel accuracy performance of the constant pattern with different α options. We then discuss the throughput of binary pattern by comparing with one constant pattern under joint impacts of CREs.
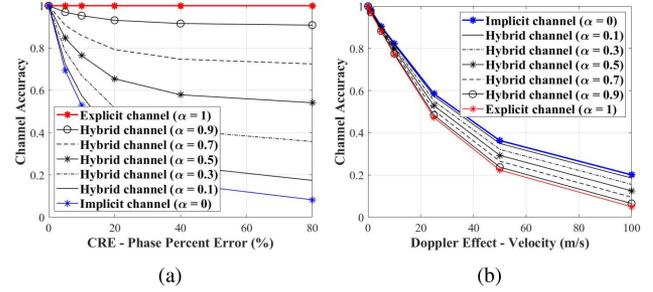
As depicted in Figure 5, we consider implementing explicit feedback that obtains explicit CSI via our proposed channel-differential feedback scheme. In addition, the implicit CSI is obtained based on the LTS field in the feedback message sent from the UE. The transmitter will and control the factor parameter α to utilize the combined explicit and implicit CSI to improve the channel accuracy. Figure 16 examines the constant pattern by evaluating how the channel accuracy performance of the hybrid feedback behaves on different α values ($\alpha \in \{0.1, 0.3, 0.5, 0.7, 0.9\}$) under two different emulated channels: Phase error and Doppler effects. Note that we compare against implicit and explicit feedback in the same figure, which correspond to the cases of $\alpha = 0$ and 1, respectively. Figure 16(a) shows that channel estimation accuracy of the hybrid feedback scheme increases with increasing α parameters, assuming the same CRE levels. For example, an α of 0.1 leads to a channel accuracy approaching the performance of implicit CSI. However, as α continues to increase, the channel accuracy of the associated α increases significantly: an α of 0.9 outperforms an α of 0.1 by 465% in channel estimation quality. Figure 16(b) shows increasing Doppler velocity significantly degrades the channel accuracy, while a larger α is more susceptible to Doppler effects. For example, a Doppler velocity of 100 m/s can lead to channel accuracy of 0.11 at α of 0.9, and channel accuracy of 0.24 at α of 0.1. Our evaluation demonstrates that implicit feedback is susceptible to CRE, while explicit feedback is more affected by Doppler effects. We believe these results impact future implementation of hybrid feedback based on practical channel conditions.

Then, we explore the throughput gain for each constant α choice to find the option that leads to the highest throughput gain. To do so, we use repeatable experiments to create the random samples of channel coherence and CRE using a channel emulator. By performing hybrid feedback with different α options, the channel estimates are predicted and calibrated to throughput estimates with consideration of training overhead. Our evaluation shows that $\alpha = 0.5$ gives the highest throughput gain performance out of all constant options. Figure 17 presents the statistical CDF of the calibrated throughput for the best constant pattern when $\alpha = 0.5$ (only showing $\alpha = 0.3$ and 0.7 here for better comparison with $\alpha = 0.5$). We observe that $\alpha = 0.5$ results in outperforming the explicit/implicit schemes by 32%, on average. This result shows that beamforming with the
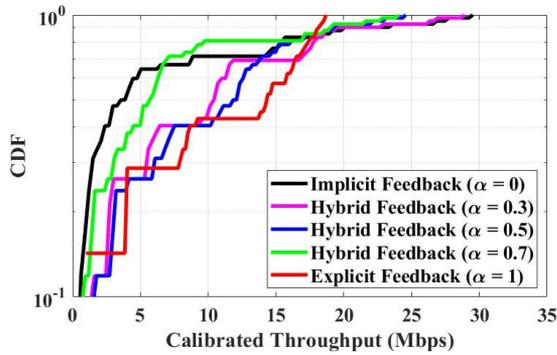
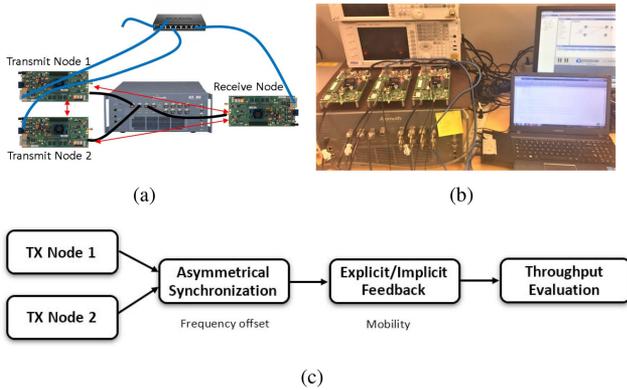Fig. 17.   CDF of Calibrated Throughput for Hybrid Feedback Mechanisms.

Fig. 18.   Experimental Setup. (a) Experimental Diagram. (b) System Emulation. (c) Feedback Analysis Flow.

proposed hybrid feedback mechanism can significantly improve throughput performance.

E. Distributed Beamforming

We extend our analysis to a distributed beamforming scheme under asymmetrical synchronization. Specifically, wireless radios are now situated on distinct transmission nodes, which have independent oscillators and amplifiers that introduce different frequency and phase offsets. This means that extra estimation error will result from oscillators mismatch. In addition, mobility of transmission nodes can, as previously explained, significantly impact the feedback schemes. Therefore, it is essential to investigate the impact of these joint factors on the performance of a distributed beamforming system.

In order to evaluate the effects of frequency offset and Doppler shift, we design and perform our experiments using an Azimuth ACE-MX channel emulator and generate a controlled and repeatable propagation channel and fading parameters. The setup for this section is shown in Figure 18. For the beamformer, we use two WARP boards and connect them with the Azimuth ACE-MX via RF cables that run from the transmission ports to the two emulator input ports. A third WARP board is used as the beamformee connected to the emulator output port. We control the channel emulator with a TCL script that generates repeatable 5-tap Rayleigh distributed samples. The channel emulator is controlled over an Ethernet cable from the control PC by the Director-II software, from which we can configure the channel
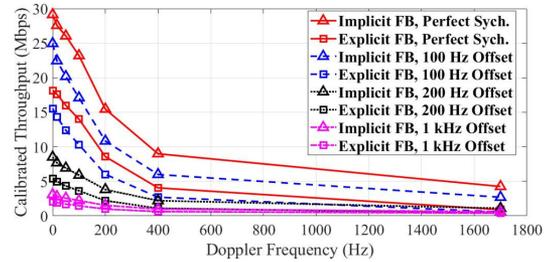

Fig. 19.   Distributed link performance analysis.

characteristics such as the distribution model, channel taps, path-loss, Doppler effects, and input/output attenuation.

We evaluate the impact of asymmetrical synchronization using a software-defined radio platform, WARPLab. WARPLab enables users to implement PHY and MAC layer functionalities in MATLAB and transmit/receive actual signals using RF radios. Then, the coded and modulated data samples are transferred to the WARP board via an Ethernet cable. WARP is then triggered to transmit data samples over the air. The receiver samples the signal and then transfers the raw samples to the PC, where the receiver also leverages MATLAB to demodulate and decode the transmitted data for post-processing and data analysis. The feedback test scheme is depicted in Figure 18(c). In order to introduce an asymmetrical frequency offset for the two transmitting nodes, we introduce a shifting parameter to the digital samples with various frequency offset settings. The frequency offset is the carrier frequency difference between the distributed nodes, which can be emulated by multiplying the samples with a time-based exponential shift (sampling rate $= 40$ MHz). Since the WARP board is reported to have an a oscillator deviation of 3 ppm (15 KHz as the worst offset), we configure the frequency error to be in the range of 100 Hz, 200 Hz, and 1 KHz. Then, we evaluate the impact of mobility introduced by the channel on the frequency offset from these sources. The Doppler effect is controlled by the channel emulator. We also use an RF synchronization cable to create zero frequency offset as a reference for our evaluation.

The impact of the resulting channel and its translation to throughput are shown in Figure 19. It shows how various frequency offsets and Doppler frequencies with explicit and implicit feedback schemes can affect the calibrated throughput. We observe that, with perfect synchronization, feedback performance based on distributed MIMO can achieve the same throughput performance as a centralized MIMO scheme due to perfect channel estimation accuracy. Furthermore, the levels of frequency offset can significantly affect MIMO performance. With a frequency offset of 100 Hz, the channel accuracy drops by 10%. However, the channel accuracy significantly degrades to 80% with a frequency offset of 1 kHz. *This result shows that the frequency offset can significantly degrade the distributed beamforming link performance.*

F. Channel-Aware Feedback

Although the optimal rate for channel estimation can be evaluated by both simulation and experiments in prior work, fixed overheads have been used for each feedback operation. In our
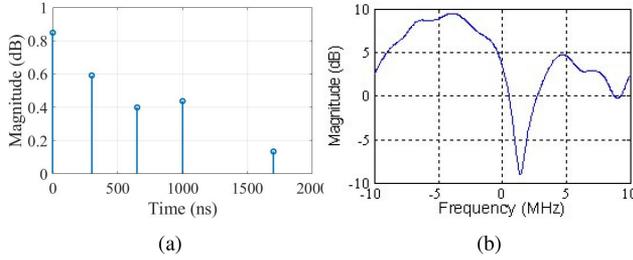
Fig. 20. 5-Tap Rayleigh Channel Model with Doppler Effects: (a) Time Domain. (b) Frequency Domain.

Fig. 21. Channel Aware feedback. (a) 32 Estimates. (b) 16 Estimates.

previous experiments, we emulated a Rayleigh fading channel with 5 taps and implemented 64 uniformly-distributed element vectors for OFDM transmissions at each transmit antenna to describe the channel properties in the frequency domain. As shown in Figure 20, the channel taps can be modeled as a Finite Impulse Response (FIR) filter with a frequency response given by:

$$\overline{h}_m(k) = \frac{1}{N} \sum_{n=-\infty}^{\infty} c(n) e^{-j2\pi nk\Delta_f}. \tag{23}$$

Here, $\overline{h}_m(k)$ represents the channel vectors (in the frequency domain) that are estimated by training overhead, depending on feedback mechanism. The FIR channel tap is $c(n)$.

We anticipate the payload of feedback will only increase as the antenna number increases for massive MIMO systems. Also, since channels can be frequency-selective or frequency-flat [35], this motivates the design of a channel-aware feedback (CAF) mechanism which dynamically implements a proportional feedback matrix based on flatness properties of channel for each transmit antenna. Assume the vector length of channel estimates is limited to set $I \in \{8, 16, 32, 64\}$ with an FFT/IFFT DSP implementation. In order to reduce training overhead while achieving satisfactory estimation performance, the predicted vector length i is derived by:

$$\arg\max_{i \in I} \{i | E(\|\overline{\mathbf{h}}_{\mathbf{i},\mathbf{m}} - \mathbf{h}_{\mathbf{m}}\|^2) < T\}. \tag{24}$$

Here, T denotes the error threshold, $\overline{\mathbf{h}}_{\mathbf{i},\mathbf{m}}$ is the least squares curve-fitted channel vector estimates based on i-length channel estimates, and $\mathbf{h}_{\mathbf{m}}$ is the pre-configured channel vectors. Specifically, after obtaining i-length channel estimates in the frequency domain, we use least squares fitting to derive 64-length fitted channel estimates and compare with the known 64-length channel vectors. With $T = 0.1$, when the channel spectrum tends to be more flat, less estimation points can be deployed to describe the channel and save feedback overhead. For example, in Figure 21(a), an error threshold of 0.073 is achieved with 32-length channel estimates for channel feedback, while Figure 21(b) shows another case that the number of required points is 16 with an error threshold of 0.089, which saves overhead by half but still ensure the quality of channel prediction.

We evaluate the performance of the CAF mechanism in the context of phase and amplitude errors, following the same experimental setup in Section V-A. The results are shown in
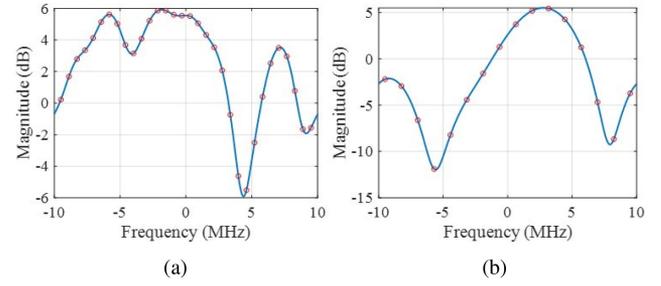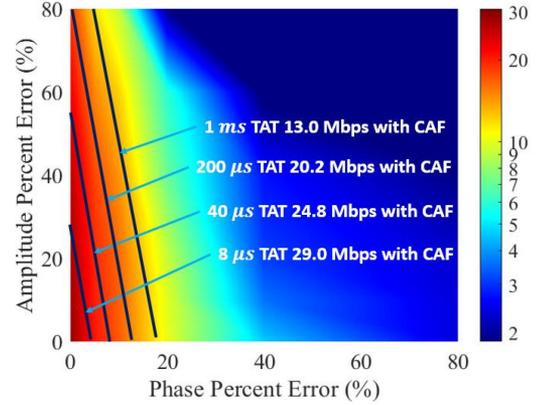

Fig. 22. CAF Mechanism Evaluation: Throughput vs. Joint Amplitude and Phase Errors.

Figure 22, where we repeat the experiments with the same Rayleigh-distributed channels for explicit/implicit channel estimation and beamforming. However, we implement a reduced feedback matrix instead of the fixed 64 vectors based on the optimal feedback vector length selection according to Equation 24. We observe that, with changing channel properties in flatness, both implicit feedback and explicit throughput increase more than that without CAF implementation by 7.3%, due to the overhead saving. Considering that an 1024 and 4096 FFT IP will be deployed as the bandwith processing increases and more flexibility will be given to feedback vector length selection, our design and concept of CAF will allow flexibility in OFDM-based WiFi and cellular network feedback design.

VI. IN-FIELD CHANNEL FEEDBACK MECHANISM EVALUATION

In this section, we perform in-field measurements to characterize channel reciprocity for air-to-ground propagation channels and evaluate the link performance of beamforming. We also experimentally explore the optimal channel update rate for channel feedback. This section serves as an application to our channel emulator experiments discussed in the previous section. We provide in-field measurements that help us understand how channel feedback and estimation accuracy are affected by velocity and reciprocity errors as well as update rate for channel estimation.

A. In-Field Channel Reciprocity Evaluation

The channel reciprocity assumption could be ill-suited for air-to-ground channels due to the severe mismatch in the height
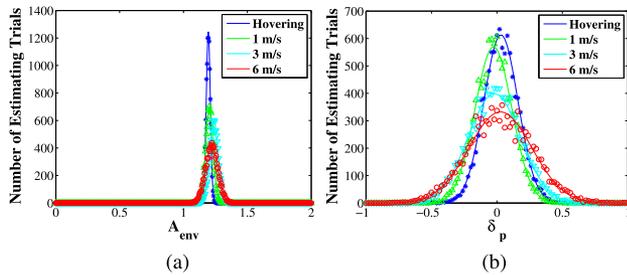
Fig. 23. Distribution Analysis for CRE. (a) Amplitude. (b) Phase Gradient.

TABLE III
STATISTIC PARAMETERS OF CHANNEL RECIPROCITY ERROR RESULTS

Case	Frequencies	Mean(A_m)	Std(A_m)	Mean(δ_p)	Std(δ_p)
Hovering	900 MHz	1.19	0.016	0.031	0.13
	1800 MHz	1.06	0.029	-0.045	0.17
	5 GHz	0.85	0.038	-0.034	0.19
1 m/s	900 MHz	1.20	0.029	-0.026	0.14
	1800 MHz	1.07	0.033	-0.034	0.19
	5 GHz	0.85	0.039	-0.028	0.26
3 m/s	900 MHz	1.23	0.033	-0.019	0.20
	1800 MHz	1.10	0.036	0.028	0.25
	5 GHz	0.81	0.043	-0.026	0.26
6 m/s	900 MHz	1.22	0.048	0.027	0.24
	1800 MHz	1.16	0.057	-0.026	0.26
	5 GHz	0.79	0.059	0.016	0.29

Fig. 24. Throughput of beamforming system with channel reciprocity.

of the communicating nodes and the susceptibility to severe channel fading with high levels of mobility. Therefore, we design baseline experiments using the UABeam system (as further described in [25]) to explore and validate the performance of both feedback methods. To clearly demonstrate the effect of channel reciprocity, we first evaluate the relationship between the DL CSI h_m and UL CSI $\bar{h}_m$. Then, we investigate the throughput performance in both the hovering and encircling scenarios introduced in Section IV-B. We capture the channel information mismatch between the UL and DL channel measured on consecutive forward and reverse traffic exchanges by defining the CRE, given by Equation (6).

During our experiments, the measured CRE results represented by amplitude and phase errors, are calculated as a function of the subcarrier obtained from every single sample measurement in both hovering or encircling experiments. In addition to the WiFi carrier frequency (5 GHz) used in the previous section, we implement feedback mechanisms across two cellular bands (900 MHz and 1800 MHz). Based on the obtained/measured CRE results, we extract the key parameters in the reciprocal error expression (7) using a minimum mean-square error (MMSE) criterion.

Figure 23 depicts a histogram in the form of four lines (superimposed to compare them) for each experiment for the different transmitting-drone velocities at 900 MHz. To form the histograms, the statistical distribution of parameters A_m and δ_p have bins of 0.005 and 0.02, respectively. These bins are extracted from 10 k channel samples for hovering and encircling experiments at 900 MHz. The solid line is a normally-distributed curve fit based on their mean and standard deviation. We found that A_m has a relatively-narrow spike around an amplitude value, with a 95.3% confidence interval in the range of (1.2-0.24, 1.2+0.24). However, the width of various phase gradients δ_p is closed related to the velocity of the drone. Similar results can also be found in other frequencies, as shown in Table III. *Therefore, our analysis shows that, while the amplitude error is approximately constant for both hovering and encircling experiments, the phase error for channel reciprocity highly depends on velocity.*

Beamforming systems will experience severe throughput degradation if imprecise channel feedback is obtained. As a result, we explore the impact of the CRE on the throughput of the DL conjugate beamforming system. We maintain the same experimental setup as before and have distinguished the DL data transmissions with the proposed 802.11ac explicit

channel-differential feedback from 802.11ac implicit feedback. Since implicit feedback does not necessarily require an NDP and feedback exchange, experiments with implicit feedback obtain CSI estimates based on the ACK message from the previous epoch, as shown in the timeline schedule in Figure 3(b).

We have conducted an extensive set of experiments with the following traffic pattern: a packet payload of 256 bytes and average epoch interval of 200 ms over an experimental duration of 300 s. Figure 24 shows the throughput results from a wireless experiment using DL and UL CSI for beamforming data transmissions at different frequencies and velocities. The beamforming throughput using explicit feedback (labeled Explicit FB) can increase the throughput by 67.8%, 93.2%, and 103.9% over that using implicit feedback (labeled Implicit FB) for 900 MHz, 1800 MHz, and 5 GHz in the hovering cases, respectively. This is explained by the less feedback overhead incurred in implicit feedback while DL CSI can be inferred by the UL channel measurements in practical highly-mobile air-to-ground channels. *Compared with the impact of physical TX-RX imbalance on the channel reciprocity, which relies on hardware characteristics, the performance of in-field UAV beamforming is more susceptible to the mobility that results in out-dated CSI from explicit feedback.* The gains of explicit feedback are even greater when it comes to the encircling cases with a throughput improvement over implicit feedback of up to 92.6%, 111.6%, and 123.9% for the aforementioned frequencies, respectively. We expect even greater throughput improvement for explicit feedback with higher velocities.

B. Update Rate for Channel Estimation

Optimizing the payload size is essential to throughput improvement while maintaining high accuracy feedback
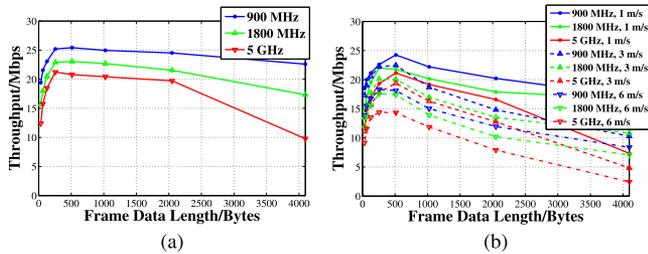
Fig. 25. Throughput for various frame lengths: (a) Hovering. (b) Encircling.

information over fading channels. In-field study ensures channel estimation under complex transmission contexts is appropriately addressed as opposed to emulated channels that rely on simplifying assumptions. We investigate the update rate for in-field airborne communications in terms of the number of OFDM symbols in a single data frame, denoted by L. First, we explore the influence of the data length on the performance of BER and throughput for a given scenario and estimate the optimal length that leads to the maximum throughput for a given carrier frequency. This also corresponds to the optimal update rate for channel estimation. Second, we examine the optimal data length across different frequencies under the same experimental context.

We now test the hovering and encircling scenarios with explicit feedback. As previously discussed, the DL CSI is fed back using our proposed approach for every data frame, but the frame data length varies. We generate the packet source with the following packet lengths: $L \in \{32, 64, 128, 256, 512, 1024, 2048, 4096\}$ with 20 MHz transmission bandwidth. Note that 4096 is the maximum payload allowed in a single data frame in the IEEE 802.11 standard.

The optimal packet length for the hovering scenario can be found in Figure 25(a). For 900 MHz and 5 GHz the optimal size is less than 512 bytes per data frame, while for 1800 MHz, the optimal size is approximately 256 bytes per frame. In Figure 25(b), the throughput decreases for the encircling scenario as drone velocity increases. However, regardless of the velocity choice, the optimal update sizes of 512 and 256 hold for their respective carrier frequencies. *These numerical results reveal that the optimal update rate for channel estimation is similar across frequencies and that a reasonable packet size for our testing system is 256 bytes across carrier frequencies.*

VII. CONCLUSION

In this work, we have examined the key factors that degrade the performance of channel reciprocity, such as transmitter-receiver imbalance, the Doppler effect due to mobility, and effective noise. First, we reviewed the current IEEE 802.11 channel feedback schemes and their challenges. Then, we presented our proposed channel feedback mechanisms to increase CSI feedback accuracy, reduce computation cost at user side, and further improve throughput, all of which have impact on future WiFi systems. Also, we evaluated implicit channel feedback and explicit feedback scheme in both emulated MIMO channels and in-field study with UAV communications. Our evaluation showed that channel estimation can be significantly affected by

channel coherence due to mobility and our proposed hybrid feedback scheme improved channel estimation accuracy and link performance by 32%. Our in-field assessment demonstrated that using optimized explicit feedback in drone-based beamforming system provided significant throughput improvement versus implicit feedback in highly-mobile air-to-ground channels.

REFERENCES

[1] J. Hoydis, S. Brink, and M. Debbah, "Massive MIMO in the UL/DL of cellular networks: How many antennas do we need," *IEEE J. Sel. Areas Commun.*, vol. 31, no. 2, pp. 160–171, Feb. 2013.

[2] J. Kim and C. Aldana, "Efficient feedback of the channel information for closedloop beamforming in WLAN," in *Proc. IEEE 63rd Veh. Technol. Conf.*, May 2006, pp. 2226–2230.

[3] E. Perahia and R. Stacey, "Next generation wireless LANs: Throughput, robustness and reliability in 802.11n," Cambridge, U.K.: Cambridge Univ. Press, Sep. 2008.

[4] L. Z. X. Zhang and A. Sabharwal, "Directional training for FDD massive MIMO," *IEEE Trans. Wireless Commun.*, vol. 17, no. 8, pp. 5183–5197, Aug. 2018.

[5] G. C. Z. Jiang, A. F. Molisch, and Z. Niu, "Achievable rates of FDD massive MIMO systems with spatial channel correlation," *IEEE Trans. Wireless Commun.*, vol. 14, no. 5, pp. 2868–2882, May 2015.

[6] L. C. W. Yang, L. Chen, and Y. E. Liu, "Super-resolution for achieving frequency division duplex (FDD) channel reciprocity," in *Proc. IEEE 19th Int. Workshop Signal Process. Adv. Wireless Commun.*, 2018, pp. 1–5.

[7] M. M. Rahman, H. E. Baidoo-Williams, R. Mudumbai, and S. Dasgupta, "Fully wireless implementation of distributed beamforming on a software-defined radio platform," in *Proc. IEEE 11th Int. Conf. Inf. Process. Sensor Netw.*, 2012, pp. 305–315.

[8] H. Lou, M. Ghosh, P. Xia, and R. Olesen, "A comparison of implicit and explicit channel feedback methods for MU-MIMO WLAN systems," in *Proc. IEEE 24th Annu. Int. Symp. Personal, Indoor, Mobile Radio Commun.*, 2013, pp. 419–424.

[9] S. Haile, "Investigation of channel reciprocity for OFDM TDD systems," Master's Thesis, Univ. of Waterloo, Canada, 2009.

[10] A. Bourdoux and J. Liu, "Transceiver non-idealities in multiantenna systems," *Smart Antennas: State of the Art*, Eurasip Book Series on Signal Processing & Communications, 2005.

[11] A. Alexiou, "Assessment of advanced beamforming and MIMO technologies," Tech. Rep. IST-2003-507581 issue 1.0, D2.7, WINNER, 2005.

[12] A. Tolli, M. Codreanu, and M. Juntti, "Compensation of non-reciprocal interference in adaptive MIMO-OFDM cellular systems," *IEEE Trans. Wireless Commun.*, vol. 6, no. 2, pp. 545–555, Feb. 2007.

[13] K. Schober and R. Wichman, "MIMO-OFDM channel estimation with eigen beamforming and user specific reference signals," in *Proc. IEEE Veh. Technol. Conf.*, 2009, pp. 1–5.

[14] R. Cepeda, M. Fitton, and A. Nix, "The performance of robust adaptive modulation over wireless channels with non reciprocal interference," in *Proc. IEEE Veh. Technol. Conf.*, 2002, pp. 1497–1501.

[15] M. Badi, J. Wensowitch, D. Rajan, and J. Camp, "Experimental evaluation of antenna polarization and elevation effects on drone communications," in *Proc. 22nd Int. ACM Conf. Model., Anal. Simul. Wireless Mobile Syst.*, 2019, pp. 211–220.

[16] A. AlHourani, S. Kandeepan, and A. Jamalipour, "Modeling air-to-ground path loss for low altitude platforms in urban environments," in *Proc. IEEE Global Commun. Conf.*, 2014, pp. 2898–2904.

[17] A. Al-Hourani, S. Kandeepan, and S. Lardner, "Optimal LAP altitude for maximum coverage," *IEEE Wireless Commun. Lett.*, vol. 3, no. 6, pp. 569–572, Dec. 2014.

[18] E. Kalantari, H. Yanikomeroglu, and A. Yongacoglu, "On the number and 3D placement of drone base stations in wireless cellular networks," in *Proc. IEEE Veh. Technol. Conf.*, 2016, pp. 1–6.

[19] Y. Zheng, Y. Wang, and F. Meng, "Modeling and simulation of pathloss and fading for air-ground link of HAPs within a network simulator," in *Proc. IEEE Int. Conf. Cyber-Enabled Distrib. Comput. Knowl. Discov.*, 2013, pp. 421–426.

[20] S. Chandrasekharan *et al.*, "Performance evaluation of LTE and WiFi technologies in aerial networks," in *Proc. IEEE Globecom Workshops*, 2016, pp. 1–7.

[21] H. Yu, L. Zhong, A. Sabharwal, and D. Kao, "Beamforming on mobile devices: A first study," in *Proc. 17th Annu. Int. Conf. Mobile Comput. Netw.*, 2011, pp. 265–276.

[22] E. Aryafar, M. Khojastepour, K. Sundaresan, S. Rangarajan, and E. Knightly, "ADAM: An adaptive beamforming system for multicasting in wireless LANs," in *Proc. IEEE INFOCOM*, Mar. 2012, pp. 1467–1475.

[23] A. H. L. U. A. BubaAbdullahi, F. S. R. Caldeirinha, and J. Eastment, "Real time multiuser-MIMO beamforming/steering using NI-2922 universal software radio peripheral," in *Adv. Inf. Commun.*, 2020.

[24] C. Codau *et al.*, "Experimental evaluation of a beamforming-capable system using NI USRP software defined radios," in *Proc. 18th RoEduNet Conf.: Netw. Educ. Res. (RoEduNet)*, 2019, pp. 1–6.

[25] Y. Shi, R. Enami, J. Wensowitch, and J. Camp, "UABeam: UAV-based beamforming system analysis with in-field air-to-ground channels," in *Proc. IEEE 15th Annu. Int. Conf. Sens., Commun. Netw.*, 2018, pp. 1–9.

[26] M. Morelli, C. C. J. Kuo, and M. O. Pun, "Synchronization techniques for orthogonal frequency division multiple access (OFDMA): A tutorial review," *Proc. IEEE*, vol. 95, no. 7, pp. 1394–1427, Jul. 2007.

[27] D. Love and R. Heath, "Limited feedback precoding for spatial multiplexing systems," in *Proc. IEEE Mil. Commun. Conf.*, 2013, pp. 627–632.

[28] T. Pande, D. J. Love, and J. V. Krogmeier, "Reduced feedback MIMO-OFDM precoding and antenna selection," *IEEE Trans. Signal Process.*, vol. 55, no. 5, pp. 2284–2293, May 2007.

[29] Q. Wang, H. Feng, L. Cimini, L. Greenstein, D. Chan, and A. Hedayat, "Comparison of quantization techniques for downlink multi-user MIMO channels with limited feedback," *IEEE Wireless Commun. Lett.*, vol. 3, no. 2, pp. 165–168, Apr. 2014.

[30] Y. Ma, G. Zhou, and S. Lin, "Elimo: Eliminating channel feedback from MIMO," in *Proc. IEEE Int. Conf. Smart Comput.*, 2017, pp. 1–8.

[31] "WARPLab 7," [Online]. Available: http://warpproject.org/trac/wiki/WARPLab

[32] "Hackfest Wireless Channel Emulator," [Online]. Available: https://cdn.thomasnet.com/ccp/30260278/72353.pdf

[33] B. Siva, K. Reddy, and L. Boppana, "Concatenated coding in OFDM for WiMAX using USRP N210 and GNU radio," *Int. J. Wireless Mobile Netw.*, vol. 5, pp. 55–68, 2013.

[34] E. Blossom, "Exploring GNU Radio," in Gnu.org, 2012.

[35] Y. Du, Y. Shi, E. Aryafar, P. Cui, J. Camp, and M. Chiang, "SAMU: Design and implementation of selectivity-aware MU-MIMO for wideband WiFi," in *Proc. IEEE 12th Annu. Int. Conf. Sens., Commun., Netw.*, 2018, pp. 229–237.

Mahmoud Badi received the B.S. degree in electrical and electronics engineering from the University of Tripoli, Tripoli, Libya, in 2012 and the M.S. degree in telecommunications from Southern Methodist University (SMU), Dallas, TX, USA, in 2017. He is currently working toward the Ph.D. degree in electrical and computer engineering with SMU. His current research interests include UAV communications and centralized and distributed multiple antenna systems. He was the recipient of Fulbright scholarship for the M.S. degree.

Dinesh Rajan (Senior Member, IEEE) received the B.Tech. degree in electrical engineering from the Indian Institute of Technology, Madras, Chennai, India, and the M.S. and Ph.D. degrees in electrical and computer engineering from Rice University, Houston, TX, USA. He is currently the Department Chair and Cecil and Ida Green Professor with Electrical and Computer Engineering Department, Southern Methodist University, Dallas, TX, USA. In August 2002, he joined Electrical Engineering Department, Southern Methodist University, as an Assistant Professor. His current research interests include communications theory, wireless networks, information theory, and computational imaging. He was the recipient of the NSF CAREER Award for his work on applying information theory to the design of mobile wireless networks. He was also the recipient of the Golden Mustang Outstanding Faculty Award and the Senior Ford Research Fellowship from SMU.

Joseph Camp (Member, IEEE) received the B.S. (Hons.) degree in electrical and computer engineering from the UT-Austin, Austin, TX, USA, and the M.S. and Ph.D. degrees in electrical and computer engineering from Rice University, Houston, TX, USA. He is currently an Associate Professor of electrical and computer engineering with Southern Methodist University, Dallas, TX, USA. In 2009, he joined the SMU Faculty. His research team has performed more than 200 million in-field wireless measurements around the world via Android deployment and local characterization via drones, campus buses, vehicles, and buildings. His research interests include wireless communications and networking, crowdsourcing, and drones, specifically focused on the deployment, measurement, and analysis of large-scale systems and development of embedded protocols. He was the recipient of the National Science Foundation CAREER Award in 2012 and the Golden Mustang Teaching Award in 2014.

Yan Shi received the B.E. degree in telecommunications engineering from the Wuhan University of Technology, Wuhan, China, in 2013, the M.S. degree in electrical engineering from Baylor University, Waco, TX, USA, in 2015, and the Ph.D. degree in electrical engineering from Southern Methodist University, Dallas, TX, USA, in 2019. He is currently a Senior Wireless Systems Engineer with JMA Wireless, TX, USA. His research interests include UAV and millimeter wave communications, and beamforming in mobile systems.